UDK 669.018.2:66.040
Original scientific article/Izvirni znanstveni članek

ISSN 1580-2949
Mater. Tehnol.

TAILORING THE MECHANICAL PROPERTIES OF PBF-LB/M INCONEL 718 THROUGH POST-PROCESSING: HIP AND HEAT TREATMENTS

OPTIMIZACIJA MEHANSKIH LASTNOSTI INCONELA 718, IZDELANEGA Z METODO PBF-LB/M, S POSTOPKI NAKNADNE OBDELAVE: HIP IN TOPLOTNA OBDELAVA

Črtomir Donik[1*], Irena Paulin[1], Bojan Podgornik[1], Borut Žužek[1], Federico Uriati[2], Katrin Wudy[3], Matjaž Godec[1]

[1]Institute of Metals and Technology, Ljubljana, Slovenia
[2]BEAMIT SpA, Fornovo di Taro, Italy
[3]Technical University of Munich, Munich, Germany

Prejem rokopisa – received: 2025-05-17; sprejem za objavo – accepted for publication: 2025-05-26

doi:10.17222/mit.2025.1457

Inconel 718 (IN718) is a nickel-based superalloy that is extensively utilised in the aerospace, automotive, nuclear, and power-generation industries, primarily due to its exceptional high-temperature strength, fatigue and creep resistance, corrosion resistance, and superior weldability. These properties result from optimised thermal and mechanical processing. PBF-LB/M-produced IN718 exhibits characteristic microstructural defects and residual stresses that limit its mechanical properties. The current study systematically examines the effects of various critical post-processing treatments, including stress-relief annealing, Hot Isostatic Pressing (HIP), solution annealing, and ageing treatments, on the microstructure and mechanical properties of PBF-LB/M-manufactured IN718. Furthermore, different combinations of these processes are analysed to explore the potential synergistic benefits, with the possibility of omitting some post-treatments during AM-prepared IN718. The microstructural evolution is investigated using scanning electron microscopy (SEM), complemented by comprehensive mechanical testing, including tensile and hardness tests. The results provide a deeper understanding of the relationship between specific post-processing routes and their impacts on the mechanical performance, supporting the development of optimised treatment strategies for the enhanced reliability and service life of AM-fabricated IN718 components.

Keywords: PBF-LB/M, IN718, SEM, post-processing-heat treatment, mechanical properties

Inconel 718 (IN718) je superzlitina na osnovi niklja, ki se pogosto uporablja v letalski, avtomobilski, jedrski in energetski industriji, predvsem zaradi svoje izjemne trdnosti pri visokih temperaturah, odpornosti proti utrujenosti in lezenju, odpornosti proti koroziji ter odličnih varilnih lastnosti. Želene lastnosti so posledica optimiziranih toplotnih in mehanskih postopkov obdelave. PBF-LB/M proizveden IN718 kaže značilne mikrostrukturne napake in preostale napetosti, ki omejujejo njegove mehanske lastnosti. Ta študija sistematično preučuje učinke različnih ključnih postopkov naknadne obdelave, vključno z žarjenjem za odpravo napetosti, vročim izostatskim stiskanjem (HIP), raztopinskim žarjenjem in postopki staranja, na mikrostrukturo in mehanske lastnosti PBF-LB/M izdelanega IN718. Poleg tega so analizirane različne kombinacije teh procesov, da se raziščejo morebitne sinergijske koristi, pri čemer se upošteva možnost izpuščanja nekaterih naknadnih obdelav pri AM pripravljenem IN718. Razvoj mikrostrukture se preiskuje z vrstično elektronsko mikroskopijo (SEM), ki jo dopolnjujejo celovita mehanska testiranja, vključno s testi natezne trdnosti in trdote. Rezultati zagotavljajo globlje razumevanje odnosa med specifičnimi postopki naknadne obdelave in njihovimi vplivi na mehansko učinkovitost, kar podpira razvoj optimiziranih strategij obdelave za povečano zanesljivost in življenjsko dobo AM izdelanih komponent IN718.

Ključne besede: PBF-LB/M, IN718, SEM, naknadna obdelava-toplotna obdelava, mehanske lastnosti

1 INTRODUCTION

Inconel 718 (IN718) is a popular nickel-based superalloy that is extensively utilised in the aerospace, automotive, nuclear, and power-generation industries, primarily due to its exceptional high-temperature strength, fatigue and creep resistance, corrosion resistance, and superior weldability.[1] Recently, additive manufacturing (AM), particularly the Laser Powder Bed Fusion (PBF-LB/M) process, has revolutionised the production of IN718 components by enabling complex, near-net-shape geometries that were previously challenging or impossible through conventional manufacturing methods, thus reducing material waste and facilitating innovative component designs.[2–4] Despite its many advantages, the PBF-LB/M process introduces characteristic microstructural features, including columnar grains, precipitates, and internal porosity, as well as substantial residual stresses.[5–8] These defects and stresses adversely influence the mechanical properties, fatigue life, and overall performance of the fabricated components, emphasising the importance of optimised process parameters and post-processing treatments.[9,10]

*Corresponding author's e-mail:
crtomir.donik@imt.si

It is often desirable to keep the parts produced via PBF-LB/M in the as-built condition to reduce post-processing costs and shorten lead times. However, for many alloys, it is necessary to include post-processing and heat-treatment phases, as these can significantly enhance the final properties of the material when properly applied. The ability to investigate, control, and fine-tune the mechanical properties through specific post-processing operations is crucial for achieving the desired performance. Selecting the appropriate treatment combination for the intended application also helps to avoid redundant or unnecessary steps. The microstructure of IN718 in the as-built condition depends on the processing parameters. However, it is typically fine-grained under optimal processing conditions with dendrites and nano-dendrites oriented along the build or heat-dissipation direction. According to Shi et al.,[11] these segregations primarily involve Nb, Mo, Ti, and C, which accumulate in the interdendritic regions and along the cell boundaries, influencing subsequent phase transformations and mechanical properties. A γ-phase matrix reinforces the IN718 microstructure with two types of precipitates, i.e., γ-Ni3(Al,Ti) and γ-Ni3N, this contributes to both room-temperature and high-temperature strengthening of this alloy.[11,12] The properties of IN718 strongly depend on the PBF-LB/M-process parameters, which influence the solidification and the microstructure, through Nb, Mo, Ti, and C elements.[11,13] Micro-segregations stabilise the formation of specific phases, including the Laves phase and MC-type carbides.[14–16] The Laves phase, represented as (Ni,Fe,Cr)2(Nb,Mo,Ti), is known for its brittleness, which makes it particularly problematic, as it negatively impacts on the mechanical properties such as strength and fracture toughness.[16] According to Wang et al.,[17] the Laves phase serves as a source for crack initiation and propagation, as well as being a primary site for microvoid formation under tensile stress. On the other hand, heat treatment at temperatures above 1050 °C results in recrystallisation and grain growth, accompanied by the additional growth of MC carbide. Nevertheless, post-processing treatments remain indispensable for achieving the desired mechanical properties by relieving residual stresses and refining the microstructure of PBF-LB/M-manufactured IN718 components. Typical post-processing methods include stress-relief (SR) annealing, Hot Isostatic Pressing (HIP), solution annealing (SA), and ageing treatments. Each of these processes significantly alters the microstructure, affecting grain size, phase distribution, and mechanical properties such as the tensile strength, yield strength, hardness, and fatigue life.[5,11,18] Recent studies further emphasise the optimisation of post-processing sequences to maximise the mechanical performance and reliability.[19–23] Consequently, achieving the intended microstructure and mechanical characteristics with optimised post-processing heat and HIP treatment[18,23] is essential.

Recent advances in beam shaping and optimised laser-beam parameters have attracted substantial research interest, aiming to reduce defects and enhance the microstructure and mechanical properties of PBF-LB/M-fabricated IN718 parts[24,25] Studies have shown that novel beam-shaping strategies and optimised laser parameters effectively control the thermal gradients and solidification rates, significantly influencing grain size, morphology, and defect formation. Optimising these parameters provides new opportunities to tailor the microstructure directly during the AM process, potentially reducing the dependency on extensive post-processing.

Hot Isostatic Pressing (HIP) is commonly used in printed materials to reduce the microporosity, significantly affecting the mechanical properties. This paper systematically investigates the influence of several critical post-processing treatments on PBF-LB/M-produced IN718: stress relief annealing at 975 °C for 30 min, HIP at 1160 °C for 3 h, solution annealing at 954 °C for 1 h, and ageing treatments at 718 °C followed by 621 °C for 8 h each. Different combinations of these post-processing methods are also examined to evaluate possible synergistic effects on the microstructural refinement and mechanical performance enhancement.

Comprehensive microstructural analysis uses scanning electron microscopy (SEM), and detailed mechanical testing, including tensile and hardness measurements. The objective is to reveal the interdependence between selected post-processing routes and the resulting mechanical properties, ultimately aiding the optimisation of AM-produced IN718 components for demanding engineering applications.

2 MATERIALS AND METHODS

2.1 Material

The samples were produced using an EOS M290 system, employing process parameters set for a 40-µm layer thickness described in **Table 1**. These parameters are proprietary to the manufacturer and cannot be disclosed. However, the volume energy density (VED), which represents the amount of energy the laser delivers to the powder bed, is reported. VED is calculated using the following formula:

$$VED = \frac{P}{L \cdot S \cdot H}$$

Where: P = Laser power [W], L = Layer thickness [mm], S = Scan speed [mm/s], H = Hatch distance [mm], VED = Volume Energy Density [J/mm^3]

Table 1: The VED value for the Gaussian beam profile used:

Beam Shape	Layer Thickness [mm]	Volume Energy Density [J/mm^3]
Gaussian	0.04	67.5

2.2 Post-processing parameters with heat treatment and HIP

The heat treatments applied to the samples were carefully selected based on the general requirements outlined in international standards, as detailed in **Table 2** for easy reference. Stress Relief – 975 °C 30 min: to enhance the integrity of the components, a short thermal cycle was specifically applied to reduce the residual stresses present in the parts. This step is crucial as it also facilitates the removal of the parts from the build platform without causing damage or further complications. Hot Isostatic Pressing (HIP) – 1160 °C 3h at 100 MPa: this process was performed in accordance with the ASTM F3055 specifications, particularly in sections 13.1 and 13.1.1[26] using Quintus Technologies QIH 60. The method adheres to rigorous industry standards to ensure optimal results (reference ASTM F3055). Solution Treatment (954 °C 1h) and Ageing (718 °C 8 h followed by 621 °C 8 h): This treatment was carried out by closely following the guidelines presented in the document referenced as AMS 2774.[27] This reference is integral to ensuring that the treatment process meets the established quality requirements (ref AMS 2774).

Table 2: Processing parameters of the samples (ageing and solution annealing performed in a vacuum, and cooling with nitrogen gas)

Samples	Processed
S1	as built (AB)
S2	stress relief (SR) (975 °C 30 min)
S3	SR + HIP (1160 °C 3h at 100 MPa)
S4	SR + HIP + aging (718 °C 8 h followed by 621 °C 8 h)
S5	SR + HIP + solution annealing (SA) (954 °C 1h)
S6	SR + HIP + SA +aging
S7	SR + SA
S8	SR + SA + aging

2.3 Microstructure Characterisation

Scanning electron microscopy (SEM) equipped with a backscattered electron detector was utilised for microstructure characterisation. Metallographic samples were prepared by embedding them in conductive Bakelite resin, followed by sequential grinding and polishing with 3-µm and 1-µm diamond paste for 15 min, with an additional final 30 minutes of polishing using colloidal silica nanoparticles (OPS). For the EBSD analyses, we employed a ZEISS CrossBeam™ 550 FIB SEM system, equipped with an EDAX Hikari Super EBSD camera and EDAX APEX™ 3.0 software. This configuration enabled detailed characterisation through secondary-electron (SE) and backscatter imaging (BS), allowing us to gather both compositional and crystallographic data. Analytical parameters were carefully optimised, with SE, backscattered electron (BSE), and EDS mapping analyses conducted at a 15 kV accelerating voltage and a probe current of 2.0–5.0 nA for SE and BS.

2.4 Mechanical Analysis

From the as-built and heat-treated cylindrical blocks, standard tensile bar specimens (type B, ϕ 6 mm × 30 mm; **Figure 1**) were machined and tested at room temperature according to the standard ISO 6892-1:2019, using the A224 testing method. Yield strength, ultimate tensile strength and elongation at fracture were determined for each specimen and the average values were calculated.

Hardness test measurements were performed using a Vickers hardness tester, Falcon 800GZ, following the EN ISO 6507-1:2023 standard. Tensile tests were conducted using a Zwick Roell Kappa DS 50 kN.

Vertical cylinders were built for post-processing heat-treatment optimisation for mechanical and microstructural characterisation with bidirectional hatching and a rotation angle of 67°. A total of 24 cylinders, three for each post-processing, were printed to evaluate both the as-built and heat-treated microstructural and mechanical properties. Before mechanical testing, the cylinders were machined to the geometry of tensile bar specimens following the ISO 6892-1:2019 standard.

3 RESULTS

Figure 2 shows the microstructures of IN718 in the as-built condition (AB), using a scanning electron microscope (SEM) in the polished state with a backscattered electron (BE) detector, under various heat treatments combined with or without the HIP process. The left column of images presents lower magnifications, presenting larger areas, highlighting the grain size and morphology, while the right column shows the same samples at higher magnifications, where finer structural details are visible.

Figure 2a shows the microstructure in the AB condition, without any heat treatment or post-processing. At lower magnification, dendrites and nanodendrites are visible, and they are inclined up to 45° from the build di-

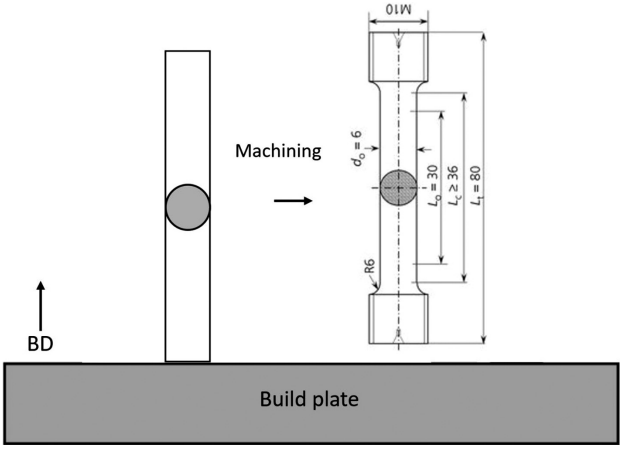

Figure 1: Sketch showing the arrangement of cylindrical blocks on the build plate from which standard tensile bar specimens were machined (BD – build direction)

rection. This is primarily due to heat dissipation during AM in that direction. The processing parameters are selected to promote the nucleation of new grains with each laser pass, thus minimizing the epitaxial growth and preventing columnar grain formation. At higher magnification, a cellular structure can be observed. In regions where elements such as Nb, Mo, and others segregate, the formation of the Laves phase occurs. According to[14,17], Nb segregation during rapid solidification leads to the precipitation of the brittle Laves phase in these interdendritic regions. Furthermore, within the Laves phase, fine carbides are also present, as noted by [15,16], who reported that nano-sized carbides precipitate within or near Laves-phase particles during solidification. The Laves phase appears exclusively at the cell boundaries, predominantly at triple junctions, and does not form a continuous network; it is fine, typically ranging in size from 10 nm to 50 nm. In **Figure 2a**, the Laves phases are indicated by arrows.

Residual stresses (RS) are relieved when as-built samples are subjected to stress relief at temperatures of 975 °C for 30 min (**Figure 2b**). The applied time and temperature are still too low to initiate recrystallization, which is evident from the lower-magnification image, where the original grain structure remains practically unchanged. However, a higher magnification reveals that the cellular structure has been eliminated, with most of the Laves phase dissolved. In these regions, enriched with elements such as Nb and Mo, the delta phase (δ-phase)[14] precipitates in needle-like structures, primarily along grain or sub-grain boundaries.[23] In the image, the δ-phase precipitates are indicated by arrows.

In the case of SR and HIP treatment at 1160 °C for 3 h, (**Figure 2c**), recrystallization and grain growth occur. The needle-like delta phase is not present even at higher magnifications in the microstructure. However, individual carbides of the MC type are observed, which, due to their sharp edges and a notch effect, are generally undesirable in the microstructure, especially when they appear in larger clusters or on chain-like structures. Additionally, the microstructure contains fine black spots, which are oxides resulting from oxygen ingress through the powder.[26,27] These oxides are also present in the as-built condition and other heat-treated states, and they do not significantly change with heat or other post-treatments. In **Figure 2c**, the oxides and carbides are marked with arrows.

In the case where the SR and HIP treatment is followed by aging at 718 °C for 8h and 621 °C for an additional 8 h (**Figure 2d**), no differences are observed in the microstructure at these magnifications compared to **Figure 2c**. The only change that can be observed just with TEM is the precipitation of γ' and γ''-phases, which are uniformly distributed within the matrix and serve to strengthen the IN718 alloy.[12]

When the SR process is combined with HIP and solution annealing (SA) at 954 °C for 1h (**Figure 2e**), the high temperature of the HIP process induces recrystallization. The subsequent solution annealing, due to its relatively lower temperature, precipitates the δ-phase in Nb-rich regions, particularly where the Laves phase was previously located.

The next post-processing step is SR, combined with HIP and SA, with the addition of an aging treatment, which promotes the precipitation of γ' and γ'' phases (**Figure 2f**). In the microstructure, in addition to the features described for the previous figure, γ' and γ'' precipitates are now present, which further strengthen the matrix through precipitation hardening. And the difference is observed in the mechanical properties

The subsequent heat-treatment process involves only a combination of SR and SA (**Figure 2g**). At these treat-

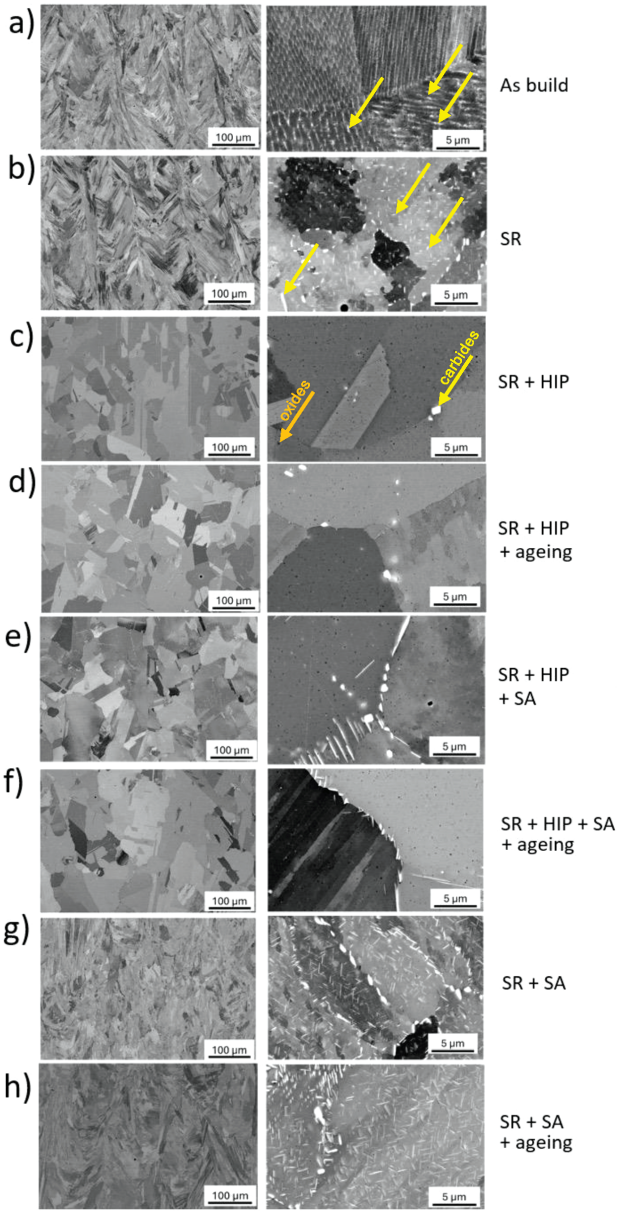

Figure 2: BS image of a) S1, b) S2, c) S3, d) S4, e) S5, f) S6, g) S7 and h) S8 sample preparation at two different magnifications

ment temperatures, recrystallization does not occur, but recovery processes take place, reducing and eliminating the dislocation substructure. The Laves phase is mostly dissolved during the stress-relief process, as its temperature is relatively high. However, since the solution annealing temperature is relatively low, a significant amount of δ-phase forms in the microstructure. The δ-phase does not contribute to matrix strengthening and a boost to mechanical properties; its detrimental effect lies in the fact that it consumes niobium (Nb), which would otherwise be available for forming γ' and γ'' precipitates during ageing.

In the case of SR and SA with the addition of an aging process (**Figure 2h**), no visible differences can be observed in the microstructure at these magnifications in the SEM. These differences become apparent only through TEM analysis, where γ' and γ'' precipitates are present within the matrix, contributing to precipitation strengthening. In both images, δ-phases and carbides are indicated by arrows. Under these heat-treatment conditions, the carbides are predominantly of the $M_{23}C_6$ type, as reported by [11,12,14,16], who observed that prolonged exposure to intermediate temperatures promotes the formation of chromium-rich $M_{23}C_6$ carbides along grain boundaries in IN718.

In addition to the microstructural characterisation, static mechanical tests were conducted on all the specimens. The results, summarised in **Figure 3**, clearly illustrate the significant impact of different heat-treatment strategies on the mechanical behaviour of the IN718 alloy. The sample treated with SR, HIP, and SA exhibited the lowest yield and tensile strengths of all the tested conditions. Despite this reduction in strength, this specimen demonstrated a notably high elongation (A) and reduction of area (Z), indicating superior ductility due to recrystallisation, Nb not in γ-phases, and the elimination of residual stresses. Following this, the AB sample and the sample subjected solely to SR showed comparable values of yield and tensile strength, suggesting that stress relief alone does not significantly influence the static strength properties relative to the as-built condition. However, a distinct increase in elongation was observed in the SR sample, attributed to the partial elimination of the dislocation substructure and recovery processes occurring at elevated temperatures, without triggering recrystallisation. The specimen subjected to both SR and SA exhibited mechanical strength similar to that of just the SR sample, but with slightly lower elongation characteristics. This improvement in ductility is primarily due to the dissolution of Laves phases and the complete removal of dislocation structures during SA. Furthermore, an additional heat-treatment sequence, consisting of SR followed by HIP, but without aging, was applied to another sample. This treatment led to material densification and induced recrystallization. As a result, an increase in both the yield and tensile strengths was recorded compared to previous treatments. However, this enhancement in strength was accompanied by a reduction in A and Z, primarily due to grain growth and the complete elimination of the characteristic as-printed microstructure.

The application of aging enhanced the mechanical properties of the investigated IN718 samples, primarily due to the precipitation of the strengthening γ' and γ'' phases. All three aged samples exhibited superior yield and tensile strength values compared to non-aged conditions. However, as expected, the aging process resulted in a marked decrease in ductility, evidenced by reduced values of A and Z across all specimens. Among the aged samples, the specimen subjected to SR, HIP, solution annealing with aging demonstrated the lowest strength values. This reduction in mechanical performance is attributed to the partial formation of δ-phase precipitates along grain boundaries during SA, which adversely affects the precipitation hardening mechanism by depleting critical alloying elements such as Nb and Mo. In contrast, the best mechanical performance was observed in samples treated with SR, HIP with aging and SR, SA with aging, without HIP. The key difference between these two treatments lies in their distinct microstructural evolution. The sample treated with HIP underwent recrystallization, which, in the absence of δ-phase formation, facilitated a higher volume fraction of γ' precipitates, thereby enhancing strength. Additionally, the HIP process contributed to improved densification, which positively influenced ductility, as reflected by higher A and Z values. Conversely, the non-HIP sample preserved a fine-grained microstructure, which typically promotes higher strength due to grain-boundary strengthening. However, the extensive precipitation of δ-phase in this condition reduced the amount of γ'-phase, thereby limiting the overall strengthening potential. Despite this limitation, the fine-grain size provided a favorable balance between strength and ductility, although ductility remained lower compared to the HIP-treated counterpart.

The measured hardness values correlate closely with the applied heat-treatment routes and the associated microstructural evolution of the PBF-LB/M-produced IN718 samples. In the as-built condition, the hardness was recorded at approximately 350 HV10, primarily due to the presence of a high dislocation density and Laves phases. A slight decrease in hardness was observed following the stress-relief treatment, attributed to partial recovery and the reduction of residual stresses. The lowest hardness values were obtained in samples subjected to the HIP process followed by solution annealing, where recrystallization and the dissolution of strengthening features significantly reduced hardness. In the absence of HIP, when only solution annealing was applied, the hardness decreased to around 300 HV10, which is notably lower than that of the as-built condition. This reduction is associated with eliminating the dislocation substructure and partial dissolution of Laves phases, without the compensatory effect of precipitation hardening. Con-

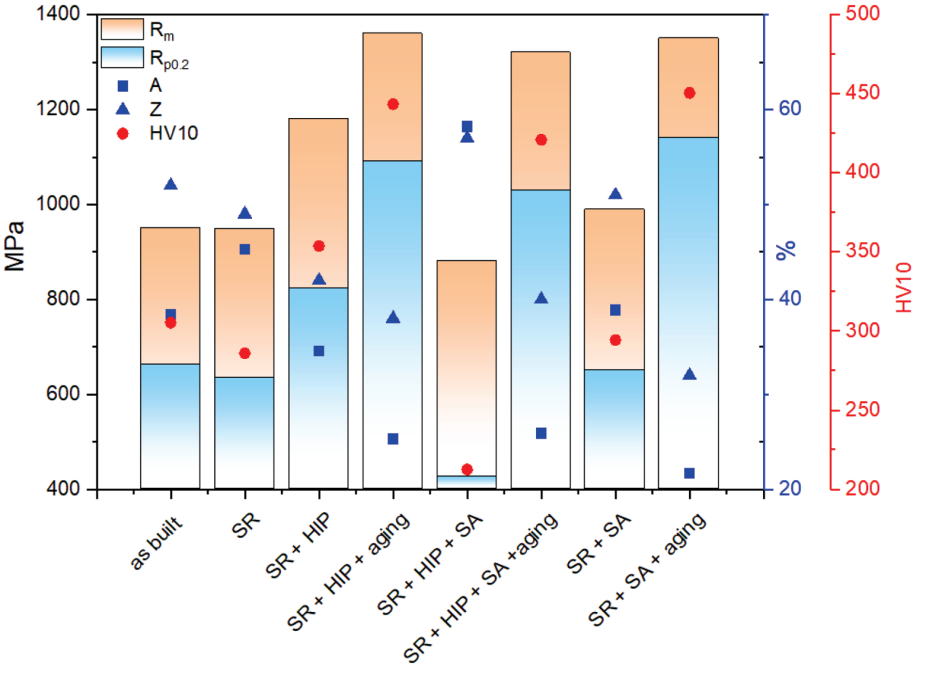

Figure 3: Mechanical properties $R_{p0.2}$, R_m, A, Z and HV10

versely, the highest hardness values were consistently achieved when aging was employed as the final step in the heat-treatment process. The peak hardness was recorded in the sample treated with SR, SA with aging, where the precipitation of γ'- and γ''-phases effectively enhanced the material's hardness despite the presence of δ-phase precipitates.

4 DISCUSSION

It is essential to control the heat-treatment process in a manner that minimizes the precipitation of the δ-phase. Although the δ-phase is not inherently detrimental, it does not contribute to matrix strengthening. Its formation depletes niobium and other alloying elements from the matrix, thereby reducing the availability of these elements for the precipitation of the γ'- and γ''-phases during aging. As a result, excessive δ-phase formation can negatively impact the overall strengthening potential by limiting γ-precipitate formation in critical areas.

The influence of γ'- and γ''-precipitates is clearly demonstrated when comparing the samples treated with *stress relief + HIP + aging* to those treated with *stress relief + HIP + solution annealing + aging*. Both treatments share identical initial steps up to the HIP process and are subsequently subjected to aging. The key difference lies in the additional solution annealing, which is performed at relatively low temperatures, promoting δ-phase precipitation along the grain boundaries. The formation of δ-phase consumes Nb, Mo, and Ti, reducing the local availability of these elements for γ'- and γ''-precipitation. This elemental depletion results in a noticeable decrease in yield strength. The comparison clearly indicates that, in this case, solution annealing is unnecessary or, alternatively, should be conducted at higher temperatures to suppress excessive δ-phase formation and preserve the precipitation potential of the γ-phases.

In cases where the HIP process is omitted, as in the *stress relief + solution annealing + aging* treatment, an increase in yield strength can be achieved due to the retention of a fine-grained microstructure, since recrystallization does not occur. The fine grain size contributes significantly to strengthening through grain-boundary hardening mechanisms. However, this approach also promotes δ-phase precipitation, which locally reduces the amount of γ'- and γ''-precipitates by consuming Nb, Mo, and Ti. While the fine grains enhance the yield strength, the presence of δ-phase limits the full potential of the precipitation hardening in affected regions.

These findings are consistent with the hardness measurements obtained for all the analyzed samples. The as-built samples exhibit intermediate hardness values, which can be attributed to the absence of γ'- and γ''-precipitates, but the presence of Laves phases and a pronounced cellular dislocation structure that contributes to material rigidity. The lowest hardness values were observed in samples subjected solely to *stress relief* or *HIP followed by solution annealing*. In these cases, the reduction in hardness is linked to the elimination of the dislocation substructure and, in the case of HIP, recrystallization. Notably, hardness values remain slightly higher when HIP is omitted due to the retention of the original fine-grained, non-recrystallized microstructure. The highest hardness was determined in the sample treated with stress relief, solution annealing, and aging.

This treatment preserved the fine-grained structure by avoiding recrystallization while promoting γ' precipitation. Although the presence of δ-phase slightly reduced the volume fraction of γ'-precipitates, combining fine grains and precipitation hardening resulted in superior hardness values.

A direct comparison between the *stress relief + HIP + aging* and *stress relief + HIP + solution annealing + aging* samples reveals that the first one exhibits slightly higher hardness values. This difference is primarily attributed to a higher volume fraction of γ'-precipitates. Since both treatments include identical initial steps and the same aging conditions, the reduced hardness in the latter is likely due to the partial formation of δ-phase during the solution-annealing step, which locally depletes the Nb and limits γ'-precipitation.

Based on these results, it can be concluded that the *stress relief + solution annealing + aging* sample exhibits slightly superior mechanical properties compared to the *stress relief + HIP + aging* sample, assuming that the reduced elongation is acceptable for the intended application. However, drawing conclusions solely from static mechanical properties can be misleading, as it is well-documented (Reference) that dynamic mechanical behavior plays a critical role in such cases. HIP processing is known to enhance the dynamic properties, such as fatigue resistance and crack propagation behavior, due to improved densification and defect elimination. Furthermore, elongation remains an important factor under dynamic loading conditions, as higher ductility can contribute to delaying crack initiation and propagation. Therefore, while static strength values may favor the non-HIP sample, the overall performance under service conditions could still be superior for the HIP-treated material.

These results underscore the critical role of optimizing heat treatment parameters, particularly in controlling δ-phase formation and leveraging the benefits of HIP, to achieve the desired combination of mechanical properties in PBF-LB/M-processed IN718 components.

5 CONCLUSIONS

A series of heat treatments, both with and without Hot Isostatic Pressing (HIP), were applied to PBF-LB/M-manufactured IN718 samples to evaluate the extent to which the material properties could be tailored. The study confirmed that aging is an essential step because it promotes the precipitation of γ'- and γ''-phases, resulting in significantly enhanced yield strength and tensile strength.

Stress relief, typically performed immediately after 3D printing – often with the parts still attached to the build plate – serves as a crucial first step in preventing warping, cracking and distortion. Elevated stress-relief temperatures also contribute to the partial dissolution of Laves phases and suppress excessive δ-phase formation.

In the context of combined heat treatments and HIP processing, the question arises regarding which treatment offers the optimal balance between mechanical performance, process efficiency, and cost-effectiveness. The selection of the most suitable procedure largely depends on the intended application of the IN718 alloy. Aging remains a critical and time-consuming step, as it is essential for achieving good mechanical properties. The formation of γ'- and γ''-precipitates is indispensable, as it significantly strengthens the material by hindering dislocation motion, particularly at elevated temperatures.[11,12] Therefore, despite efforts to simplify the processing routes, aging is considered an unavoidable stage to ensure the required performance in demanding applications.

The presented study found that performing solution annealing after the high-temperature HIP process, particularly at lower annealing temperatures, is unnecessary and even detrimental. Such a treatment promotes δ-phase precipitation, which creates depleted Nb and Mo areas, thereby reducing the potential for γ'-precipitation during subsequent aging and negatively affecting the mechanical strength.

Importantly, the presented study highlights the risks of relying solely on static mechanical properties when optimising heat-treatment routes. Although specific non-HIP treatments may exhibit comparable or even better static strength, the HIP process notably improves ductility (elongation), which is critical for dynamic performance. Enhanced elongation indicates improved fatigue resistance and a greater ability to withstand cyclic loading. Therefore, despite its higher cost, the HIP process remains a valuable step for applications where dynamic mechanical properties are of primary concern.

All these observations highlight the complex interplay between heat treatment parameters, microstructural evolution, and the resulting mechanical properties of PBF-LB/M-produced IN718 alloy.

Acknowledgement

This work was funded by the EU Research and Innovation funding programme Horizon Europe (project InShaPe - Green Additive Manufacturing through Innovative Beam Shaping and Process Monitoring, Project No. 101058523).

6 REFERENCES

[1] T. M. Pollock, S. Tin, Nickel-Based Superalloys for Advanced Turbine Engines: Chemistry, Microstructure and Properties, J Propuls Power 22 (**2006**) 361–374. doi:10.2514/1.18239

[2] T. DebRoy, H. L. Wei, J. S. Zuback, T. Mukherjee, J. W. Elmer, J. O. Milewski, A. M. Beese, A. Wilson-Heid, A. De, W. Zhang, Additive manufacturing of metallic components – Process, structure and properties, Prog Mater Sci 92 (**2018**) 112–224. doi:10.1016/j.pmatsci.2017.10.001

[3] D. Herzog, V. Seyda, E. Wycisk, C. Emmelmann, Additive manufacturing of metals, Acta Mater 117 (**2016**) 371–392. doi:10.1016/j.actamat.2016.07.019

[4] G. M. Volpato, U. Tetzlaff, M. C. Fredel, A comprehensive literature review on laser powder bed fusion of Inconel superalloys, Addit Manuf 55 (**2022**). doi:10.1016/j.addma.2022.102871

[5] P. Promoppatum, S.-C. Yao, Influence of scanning length and energy input on residual stress reduction in metal additive manufacturing: Numerical and experimental studies, J Manuf Process 49 (**2020**) 247–259. doi:10.1016/j.jmapro.2019.11.020

[6] B. N. Yadav, D.-W. Lin, M.-C. Lin, Y.-J. Tseng, H.-W. Yen, X. Van Tran, P.-C. Lin, Implemented in-situ heat treatment process for controlling the residual thermal stresses during the fabrication of Ti-6Al-4V titanium alloy through additive manufacturing, Mater Lett 356 (**2024**) 135580. doi:10.1016/j.matlet.2023.135580

[7] W. J. Sames, K. A. Unocic, G. W. Helmreich, M. M. Kirka, F. Medina, R. R. Dehoff, S. S. Babu, Feasibility of in situ controlled heat treatment (ISHT) of Inconel 718 during electron beam melting additive manufacturing, Addit Manuf 13 (**2017**) 156–165. doi:10.1016/j.addma.2016.09.001

[8] W. J. Sames, F. A. List, S. Pannala, R. R. Dehoff, S. S. Babu, The metallurgy and processing science of metal additive manufacturing, International Materials Reviews 61 (**2016**) 315–360. doi:10.1080/09506608.2015.1116649

[9] N. Martin, A. Hor, E. Copin, P. Lours, L. Ratsifandrihana, Microstructure and Mechanical Properties of Hybrid LPBF-DED Inconel 625, in: 2024: pp. 10–18. doi:10.1007/978-3-031-47784-3_2

[10] A. Tajyar, N. Brooks, N. Holtham, R. Rowe, D. J. Newell, A. N. Palazotto, K. Davami, Effects of a modified heat-treatment on microstructure and mechanical properties of additively manufactured Inconel 718, Materials Science and Engineering: A 838 (**2022**) 142770. doi:10.1016/j.msea.2022.142770

[11] J. J. Shi, X. Li, Z. X. Zhang, G. H. Cao, A. M. Russell, Z. J. Zhou, C. P. Li, G. F. Chen, Study on the microstructure and creep behavior of Inconel 718 superalloy fabricated by selective laser melting, Materials Science and Engineering: A 765 (**2019**). doi:10.1016/j.msea.2019.138282

[12] G. H. Cao, T. Y. Sun, C. H. Wang, X. Li, M. Liu, Z. X. Zhang, P. F. Hu, A. M. Russell, R. Schneider, D. Gerthsen, Z. J. Zhou, C. P. Li, G. F. Chen, Investigations of γ'-, γ"- and δ-precipitates in heat-treated Inconel 718 alloy fabricated by selective laser melting, Mater Charact 136 (**2018**) 398–406. doi:10.1016/j.matchar.2018.01.006.

[13] L. N. Carter, C. Martin, P. J. Withers, M. M. Attallah, The influence of the laser scan strategy on grain structure and cracking behaviour in SLM powder-bed fabricated nickel superalloy, J Alloys Compd 615 (**2014**) 338–347. doi:10.1016/j.jallcom.2014.06.172

[14] V. K. Singh, D. Sahoo, M. Amirthalingam, S. Karagadde, S. K. Mishra, Dissolution of the Laves phase and δ-precipitate formation mechanism in additively manufactured Inconel 718 during post printing heat treatments, Addit Manuf 81 (**2024**). doi:10.1016/j.addma.2024.104021.

[15] S. Ghaemifar, H. Mirzadeh, Precipitation kinetics of niobium carbide (NbC) during homogenization heat treatment of additively manufactured inconel 718 superalloy, Journal of Materials Research and Technology 25 (**2023**) 1774–1781. doi:10.1016/j.jmrt.2023.06.069

[16] V. Saumitra, Microstructural evolution and precipitation kinetics of carbides in L-PBF processed Inconel 718 during long-term homogenization, Mater Today Commun 42 (**2025**). doi:10.1016/j.mtcomm.2024.111192

[17] C. Wang, G. Huang, Z. Liang, X. Chen, J. Wu, T. Sun, F. Meng, S. Mironov, J. Gao, L. Zhao, X. Feng, Y. Shen, Effect of adding IN718 on crack inhibition, microstructure, and mechanical properties of selective laser melted IN738LC alloy, Opt Laser Technol 185 (**2025**). doi:10.1016/j.optlastec.2025.112600

[18] J. Radhakrishnan, S. H. Li, U. Ramamurty, Unnotched fatigue behavior of the laser powder bed fused and hot isostatic pressed Inconel 718 at 600 °C, Materials Science and Engineering: A 920 (**2025**). doi:10.1016/j.msea.2024.147527

[19] A. Sadek, Optimization of the Post-Heat Treatment of Additively Manufactured IN718, J Mater Eng Perform 33 (**2024**) 4265–4277. doi:10.1007/s11665-024-09153-8

[20] A. Dwivedi, M.K. Khurana, Y. G. Bala, S. B. Mishra, Microstructure and mechanical properties at elevated temperatures of as-built and heat-treated Inconel 718 produced through laser powder bed fusion processes, Rapid Prototyp J 31 (**2025**) 635–650. doi:10.1108/RPJ-07-2024-0293

[21] C. Chen, Z. Zhang, Y. Cai, Y. Liu, H. Chen, Research and development status of in situ field assisted laser additive manufacturing: A review, Opt Laser Technol 181 (**2025**) 111700. doi:10.1016/j.optlastec.2024.111700

[22] G. Kasperovich, J. Gussone, G. Requena, N. Schell, A. Stark, J. Haubrich, Tailoring the strength of inconel 718: Insights into LPBF parameters and heat treatment synergy, Mater Des 250 (**2025**). doi:10.1016/j.matdes.2025.113627

[23] J. Yin, D. Ma, T. Zeng, C. Wang, H. Chi, X. Li, J. Zhou, The effects of hot isostatic pressing temperature and subsequent heat treatment on the microstructure and tensile properties of laser powder bed fused IN718 nickel-based superalloy, J Alloys Compd 1020 (**2025**) 179407. doi:10.1016/j.jallcom.2025.179407

[24] N. Mirzabeigi, P. Holfelder-Schwalme, Y. He, K. Wudy, Tailored microstructure in laser-based powder bed fusion of IN718 through novel beam shaping technology, J Laser Appl 36 (**2024**). doi:10.2351/7.0001623

[25] C. Tenbrock, F. G. Fischer, K. Wissenbach, J. H. Schleifenbaum, P. Wagenblast, W. Meiners, J. Wagner, Influence of keyhole and conduction mode melting for top-hat shaped beam profiles in laser powder bed fusion, J Mater Process Technol 278 (**2020**) 116514. doi:10.1016/j.jmatprotec.2019.116514

[26] Č. Donik, J. Kraner, I. Paulin, M. Godec, Influence of the energy density for selective laser melting on the microstructure and mechanical properties of stainless steel, Metals (Basel) 10 (**2020**) 1–19. doi:10.3390/met10070919

[27] M. Godec, S. Zaefferer, B. Podgornik, M. Šinko, E. Tchernychova, Quantitative multiscale correlative microstructure analysis of additive manufacturing of stainless steel 316L processed by selective laser melting, Mater Charact 160 (**2020**). doi:10.1016/j.matchar.2019.110074